Fluid Phase Equilibria 486 (2019) 106–118

Contents lists available at ScienceDirect

Fluid Phase Equilibria

journal homepage: www.elsevier.com/locate/fluid

Prediction of phase equilibria and Gibbs free energies of transfer using molecular exchange Monte Carlo in the Gibbs ensemble

Mohammad Soroush Barhaghi, Jeffrey J. Potoff*

Department of Chemical Engineering and Materials Science, Wayne State University, Detroit, MI, 48202, USA

ARTICLE INFO

Article history:
Received 23 October 2018
Received in revised form
21 December 2018
Accepted 23 December 2018
Available online 27 December 2018

ABSTRACT

The molecular exchange Monte Carlo (MEMC) method is extended to Gibbs ensemble Monte Carlo (GEMC). The utility of the MEMC method is demonstrated through the calculation of the free energies of transfer of n-alkanes from vapor into liquid 1-octanol, n-hexadecane, and 2,2,4-trimethylpentane using isobaric-isothermal GEMC simulations. Calculations are performed for both the Transferable Potentials for Phase Equilibria (TraPPE) and Mie potentials. For all solutes, the Mie potentials predict free energies of transfer that are within 0.1 kcal/mol of experiment for solvation in n-hexadecane and 2,2,4-trimethylpentane. For TraPPE, solutes shorter than n-butane show similar agreement with experiment, but free energies for n-octane in n-hexadencane and 2,2,4-trimethylpentane are over-predicted by approximately 0.25 and 0.5 kcal/mol, respectively.

1. Introduction

The Gibbs ensemble Monte Carlo (GEMC) method, developed by Panagiotopoulos [1], provides a robust, direct method for the calculation of phase equilibria from molecular simulation. The Gibbs ensemble method uses two simulation boxes that represent a sample taken deep from within each phase. These boxes are in thermodynamic contact, and the algorithm relies on three basic movements to achieve equilibrium. These moves are configurational or conformational movement within a cell (thermal equilibration), the transfer of molecules between boxes (chemical equilibrium) and the transfer of volume from one box to the other (mechanical equilibrium).

While originally proposed as a means to simulate the vapor-liquid equilibria of Lennard-Jones spheres [1,2], numerous advances in Monte Carlo sampling methodology for the molecule swap move have been developed since its introduction, enabling GEMC to be used on increasingly complex and difficult to sample systems. The introduction of configurational-bias Monte Carlo (CBMC) sampling techniques to GEMC [3] enabled the simulation of VLE for n-alkanes up to C48 [4]. By decoupling the various intra- and inter-molecular degrees of freedom, the coupled-decoupled configurational-bias method allowed for the efficient simulations of highly branched molecules [5]. Work by Martin [6], and Sepehri et al. [7,8], focused on improving the success rate for molecule growths by using smarter methods for sampling intramolecular degrees of freedom. Methods such as, reservoir [9–11], rebridging configurational-bias [12], and self-adapting fixed end-point Monte Carlo [13] have been created that allow rings to be exchanged between simulation boxes. For systems with high densities and/or strong electrostatic interactions, which may preclude successful insertions of molecules via bead-by-bead growth, expanded ensemble methods have been developed [14–19], where a molecule is slowly deflated in one phase and inflated in another.

Martin and Siepmann suggested that by swapping the identity of molecules between phases (a “swatch” move), significant improvements in sampling could be achieved in mixtures [20]. This technique has been used in a number of studies, such as: the simulation of water [21], liquid-liquid equilibria for hexane-perfluorohexane [22], and CO_2-polymer phase behavior [23]. In previous work, our group introduced a variation of the combined swap + identity exchange (swatch) move called molecular exchange Monte Carlo (MEMC) for grand canonical Monte Carlo simulations [24]. MEMC can be thought of as a generalized version of Siepmann's swatch move, where the molecules to be exchanged do not have to share any common atom types or coordinates.

In this work, MEMC methods are presented for simulations in the Gibbs ensemble. A derivation of acceptance criteria and the algorithms for performing the MEMC move in GEMC are provided in the next section. The simulation details for determining the binary mixture phase diagrams and Gibbs free energies of transfer are provided in Simulation Methodology. In the Results and Discussion,

* Corresponding author.
E-mail address: jpotoff@wayne.edu (J.J. Potoff).

https://doi.org/10.1016/j.fluid.2018.12.032
0378-3812/

the MEMC algorithm is validated with predictions of the methane + n-butane and n-butane + perfluorobutane pressure-composition diagrams, and free energies of transfer for n-alkanes in 1-octanol, hexadecane and 2,2,4-trimethylpentane. The key findings of the work are summarized in the Conclusions.

2. Methods

In this work, the molecular exchange Monte Carlo (MEMC) method, originally developed in the context of the grand canonical ensemble, is extended to Gibbs ensemble Monte Carlo. To describe the MEMC move in the Gibbs ensemble, box 1 is assumed to be the higher density liquid phase, and box 2 is assumed to be the lower density gas phase. Attempts are made to exchange a large molecule with multiple smaller molecules in the dense phase (box 1).

For a given configuration, with N_1^L, N_2^L large and N_1^S, N_2^S small molecules in box 1 with volume V_1 and box 2 with volume of V_2, a "*deletion move*" is an attempt to remove one large molecule and insert N_{EX} small molecules inside a predefined exchange sub-volume V_{EX} in box 1. An "*insertion move*" is an attempt to remove N_{EX} small molecules, and insert one large molecule in box 1. The exchange sub-volume is defined as an orthogonal box, where the length of the box in the x-,y-, and z-dimensions can be set independently, however, in this work x = y, while z is set independently. An orthogonal sub-volume is used instead of a cube or sphere to accommodate large molecules with different aspect ratios. A heuristic for setting good values of the x-, y-, and z-dimensions is to use the geometric size of the large molecule plus 1–2 Å in each dimension. Although not used in this work, it is also possible to optimize N_{EX} and V_{EX} "on the fly" during a simulation to maximize the acceptance rate.

The acceptance criterion for a molecular exchange move that satisfies the detailed balance equation is written as

$$\mathrm{K}(old \rightarrow new) = \mathrm{K}(new \rightarrow old) \tag{1}$$

where $\mathrm{K}(i \rightarrow j)$ is the flux of probability from state i to state j. The probability flux is equal to the product of the probability of finding the system in state i, the probability of generating a move that takes state i to state j, and the probability of accepting the move:

$$\mathrm{K}(old \rightarrow new) = \mathscr{N}(old) \times \alpha(old \rightarrow new) \times acc(old \rightarrow new) \tag{2}$$

where, $\mathscr{N}(old)$ is the probability of finding the system in state *old*, $\alpha(old \rightarrow new)$ is the probability of generating a move that takes the system from state *old* to state *new*, and $acc(old \rightarrow new)$ is the probability of accepting the move that takes the system from state *old* to state *new*. Based on the detailed balance Eq. (1), the ratio of the probability of accepting the move from $old \rightarrow new$ to that of its reverse move $new \rightarrow old$ is:

$$\frac{acc(old \rightarrow new)}{acc(new \rightarrow old)} = \frac{\mathscr{N}(new)}{\mathscr{N}(old)} \times \frac{\alpha(new \rightarrow old)}{\alpha(old \rightarrow new)} \tag{3}$$

The Gibbs ensemble partition function for N distinguishable molecules and regular Cartesian (unscaled) coordinates is

$$Q_G(N,V,T) = \frac{1}{\Lambda^{3N}} \sum_{n_1=0}^{N} \int_0^V \left[\int_{v_1} exp\left[-\beta U(\boldsymbol{r}_1^{n_1}) \right] d\boldsymbol{r}_1^{n_1} \right] \times \left[\int_{V-v_1} exp\left[-\beta U\left(\boldsymbol{r}_2^{N-n_1}\right) \right] d\boldsymbol{r}_2^{N-n_1} \right] dv_1 \tag{4}$$

where, Λ is the thermal de Broglie wavelength, $N = n_1 + n_2$ is the total number of molecules in the system, n_1 is the number of molecules in box 1, n_2 is the number of molecules in box 2, $V = v_1 + v_2$ is to the total volume of the system, v_1 is the volume of box 1, v_2 is the volume of box 2, and $\boldsymbol{r}_b^i$ represents the coordinates of molecule i, in box b. The probability of finding a configuration with n_1 molecules in box 1 with volume v_1 and specific positions $\boldsymbol{r}_1^{n_1}$ and $\boldsymbol{r}_2^{N-n_1}$ is

$$\mathscr{N}\left(n_1,\ v_1,\ \boldsymbol{r}_1^{n_1}, \boldsymbol{r}_2^{N-n_1}\right) \propto exp\left\{ -\beta\left[U(\boldsymbol{r}_1^{n_1}) + U\left(\boldsymbol{r}_2^{N-n_1}\right) \right] \right\} \tag{5}$$

In both the insertion and deletion moves, the ratio of the probability of being in the configuration *new* to the probability of being in the configuration *old* is simplified to

$$\frac{\mathscr{N}(new)}{\mathscr{N}(old)} = \frac{e^{-\beta(U_1(new)+U_2(new))}}{e^{-\beta(U_1(old)+U_2(old))}} \tag{6}$$

where $\beta = 1/k_BT$, $U_1(old)$, $U_2(old)$, $U_1(new)$, and $U_2(new)$ are the potential energies of the system in configuration *old* and configuration *new* in box 1 and box 2, respectively.

The probability of generating the *new* state, for both insertion and deletion of the large molecule, is given by the product of the probability of locating the center of the exchange sub-volume at a particular point within the simulation box 1, the probability of choosing N_{EX} particular small molecules, the probability of choosing a particular large molecule, the probability of generating trial configurations for N_{EX} small molecules, and the probability of generating trial configurations for the large molecule,

$$\begin{aligned} \alpha(old \rightarrow new) = {} & P_{sub-v}(old \rightarrow new) \times P_{pick-S}(old \rightarrow new) \\ & \times P_{pick-L}(old \rightarrow new) \times P_{pos-S}(old \rightarrow new) \\ & \times P_{pos-L}(old \rightarrow new) \end{aligned} \tag{7}$$

2.1. Molecular exchange Monte Carlo, version 2 (ME-2)

For the large molecule insertion move, the geometric center of V_{EX} is placed on the centroid of a randomly selected small molecule in box 1. If the small molecule is monoatomic, the orientation of V_{EX} is assigned randomly, otherwise its z-axis is aligned with the backbone of the small molecule. For a large molecule deletion move, the geometric center of V_{EX} is located at the centroid of the selected large molecule in box 1 and its z-axis is aligned with the backbone of the large molecule. To improve acceptance rates for the MEMC move, multiple trial positions (j) and orientations (k) are performed.

Insertion of large molecule into box 1: The algorithm for the insertion of a large molecule into box 1 after the deletion of small molecule(s) is identical to ME-2 method described previously for grand canonical Monte Carlo [24]. Resolving the move requires accounting for the removal of the large molecule from box 2 and the insertion of small molecule(s) into box 2. An illustration of the large molecule insertion into box 1 in ME-2 algorithm is provided in Fig. 1.

The algorithm for doing this follows:

1. Select a large molecule out of N_2^L large molecules within the simulation box 2 with the probability of $1/N_2^L$.
2. Generate $j-1$ random trial positions for the centroid of the selected large molecule within simulation box 2 (V_2). The original position of the centroid of the large molecule will be included as the j^{th} term.

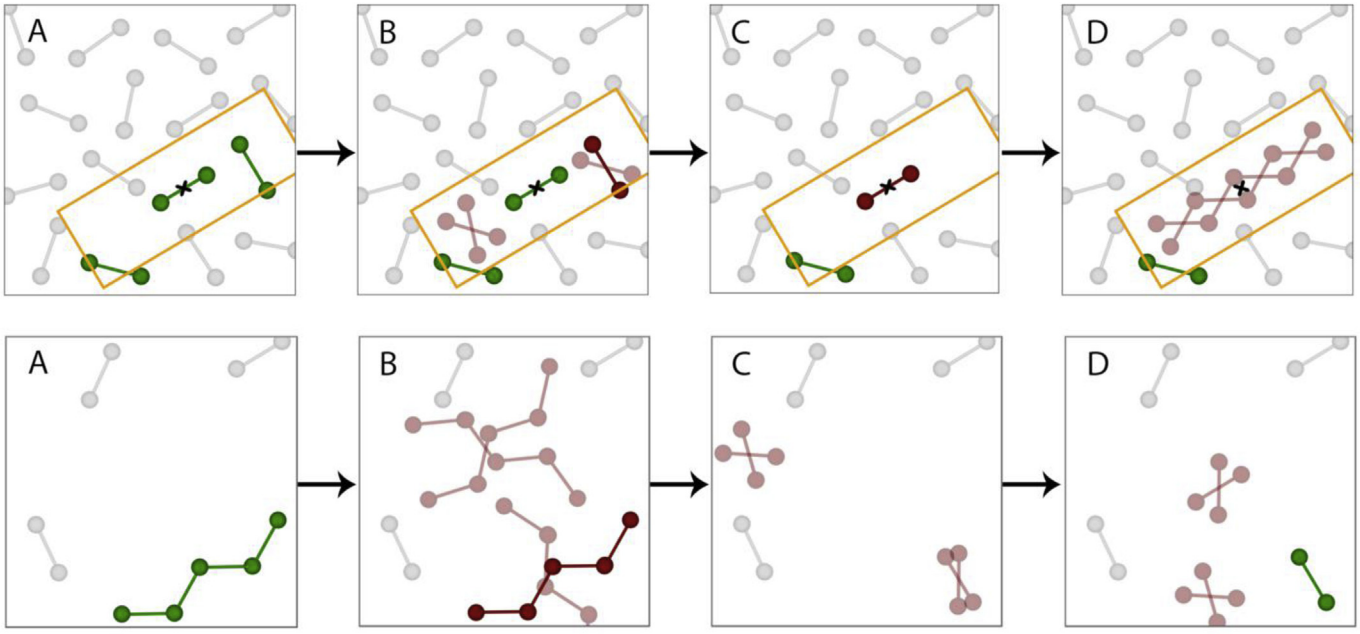

Fig. 1. Schematic for the ME-2 algorithm for the transfer of a large molecule from box 2 (gas phase) into box 1 (liquid phase), and corresponding transfer of small molecules from box 1 into box 2. Selected or inserted molecule (green), trial position (light red), and actual position of the molecule (solid red). **Top row**, represents the exchange of two small molecules with one large molecule in box 1. The sub-volume is defined by the orange box. (A) Aligning the sub-volume z-axis with the backbone of a randomly selected small molecule, with geometric center placed at centroid of the selected small molecule, identifying the small molecules within the sub-volume, and randomly picking one small molecule for transfer. (B) Generating CBMC trials (3D rotation and centroid location) for the second small molecule, and then removing it. (C) Generating CBMC 2D rotational trials around the z-axis of the sub-volume for the first small molecule and then removing it. (D) Placing the large molecule's centroid at the geometric center of the sub-volume, aligning the backbone of the large molecule with the sub-volume z-axis, performing CBMC 2D rotational trials around the z-axis of the sub-volume, and inserting it to the sub-volume. **Bottom row**, represents the exchange of one large molecule with two small molecules in box 2. (A) Selecting a random large molecule. (B) Generating CBMC trials (3D rotation and centroid location) for the selected large molecules and then removing it. (C) Generating CBMC trials (3D rotation and centroid location) for the first small molecules and then inserting it. (D) Generating CBMC trials (3D rotation and centroid location) for the second small molecule and then inserting it.

3. For each trial position p, generate k random trial orientations around the large molecule's centroid (except the j^{th} centroid, where $k-1$ random trial orientations are generated, and the original orientation of the molecule will be included as the k^{th} term). Trial orientations are generated keeping all internal degrees of freedom for the molecule fixed. The Rosenbluth weight is calculated as $W^L_{old} = \sum_{p=1}^{j}\sum_{r=1}^{k} exp(-\beta U_2^{p,r})$, where $U_2^{p,r}$ is the interaction energy of the large molecule in position p and orientation r with all other molecules in the simulation box 2.
4. Calculate the probability $P^L_{old} = \frac{exp(-\beta U_2^{j,k})}{W^L_{old}}$, where $U_2^{j,k}$ is the interaction energy of the large molecule at the original position and orientation with all other molecules in the simulation box 2. P^L_{old} is the probability of inserting the large molecule at its original configuration in the reverse move ($new \rightarrow old$). Then remove the large molecule from simulation box 2.
5. Repeat steps a→c for N_{EX} cycles ($i = 1, 2, \ldots, N_{EX}$) to insert the selected small molecules in box 2 with the probability of $N_{EX}!/V_2^{N_{EX}}$.
   a. Generate j random trial positions for the centroid of the i^{th} small molecule within simulation box 2 (V_2).
   b. For each trial position, p, generate k random trial orientations around the molecule's centroid, and calculate the Rosenbluth weight $W^S_{i,new} = \sum_{p=1}^{j}\sum_{r=1}^{k} exp(-\beta U_2^{i,p,r})$, where $U_2^{i,p,r}$ is the interaction energy of the i^{th} inserted small molecule at position p and orientation r with all the other molecules in box 2, including those added in the earlier cycles of the move.
   c. Pick one of the generated trial configurations with the probability $P^S_{i,new} = \frac{exp(-\beta U_2^{i,p,r})}{W^S_{i,new}}$ and insert the small molecule.

Deletion of large molecule from box 1: The algorithm for the deletion of a large molecule and subsequent insertion of small molecule(s) in box 1 is identical to ME-2 method described previously for simulations in the grand canonical ensemble [24]. Resolving the move requires accounting for the removal of small molecule(s) from box 2 and the insertion of the large molecule into box 2. An illustration of the large molecule deletion from box 1 in ME-2 algorithm is provided in Fig. 2.

The algorithm for doing this follows:

1. Select N_{EX} small molecule(s) out of N_2^S small molecules in the simulation box 2 with the probability of $N_{EX}!(N_2^S - N_{EX})!/N_2^S!$.
2. Repeat steps a and b for N_{EX} cycles ($i = 1, 2, \ldots, N_{EX}$) to delete the selected small molecules from simulation box 2.
   a. Generate $j-1$ random trial positions for the centroid of the i^{th} small molecule within simulation box 2 (V_2). The original position of the centroid of the i^{th} small molecule will be included as the j^{th} term.
   b. For each trial centroid position p, generate k random trial orientations around the molecule's centroid (except the j^{th} centroid, where $k-1$ random trial orientations are generated and the original orientation of the molecule will be included as the k^{th} term), and calculate the Rosenbluth

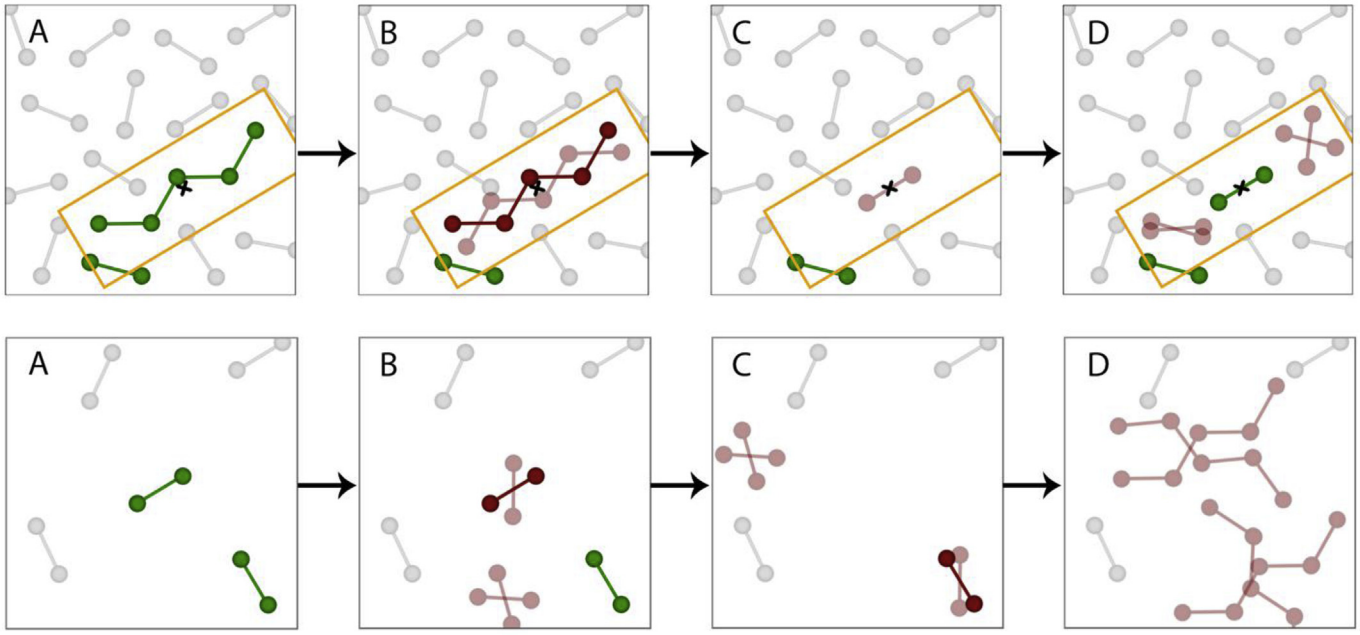

Fig. 2. Schematic for the ME-2 algorithm for transfer of a large molecule from box 1 (liquid phase) into box 2 (gas phase) and transferring two small molecules from box 2 into box 1. Selected or inserted molecule (green), trial position (light red), and actual position of the molecule (solid red). **Top row**, represents the exchange of one large molecule with two small molecules in box 1. The sub-volume is defined as the orange box. (A) Aligning the sub-volume with the backbone of the large molecule with geometric center placed at centroid of the large molecule and identifying the small molecules within the sub-volume. (B) Generating CBMC 2D rotational trials around the z-axis of the sub-volume and then removing the large molecule. (C) Placing the centroid of the first small molecule at the geometric center of the sub-volume, aligning the backbone of the small molecule with the z-axis of the sub-volume, generate the CBMC 2D rotational trials around the z-axis of the sub-volume, and then inserting it into the sub-volume. (D) Generating CBMC trials (3D rotation and centroid location) for the second small molecule and then inserting it into the sub-volume. **Bottom row**, represents the exchange of two small molecules with one large molecule in box 2. (A) Selecting two random small molecules. (B) Generating CBMC trials (3D rotation and centroid location) for the first small molecule and then removing it. (C) Generating CBMC trials (3D rotation and centroid location) for the second small molecule and then removing it. (D) Generating CBMC trials (3D rotation and centroid location) for the large molecules and then inserting it.

weight $W^S_{i,old} = \sum_{p=1}^{j}\sum_{r=1}^{k} exp(-\beta U_2^{i,p,r})$, where $U_2^{i,p,r}$ is the interaction energy of the i^{th} molecule to be removed in position p and orientation r with all other molecules in box 2, excluding those removed in the earlier cycles of the move. Finally, remove the molecule from simulation box 2. Calculate $P^S_{i,old} = \frac{exp(-\beta U_2^{i,j,k})}{W^S_{i,old}}$, where $U_2^{i,j,k}$ is the interaction energy of the i^{th} small molecule at its original centroid position and orientation with all other molecules remaining in the simulation box 2. $P^S_{i,old}$ is the probability of inserting the i^{th} small molecule back in its original configuration in the reverse move ($new \rightarrow old$).

3. Generate j random trial positions for the centroid of the selected large molecule within simulation box 2 (V_2). For each trial position p, generate k random trial orientations around the large molecule's centroid.
4. Calculate the Rosenbluth weight $W^L_{new} = \sum_{p=1}^{j}\sum_{r=1}^{k} exp(-\beta U_2^{p,r})$, where $U_2^{p,r}$ is the interaction energy of the inserted large molecule in position p and orientation r with all other molecules in simulation box 2.
5. Select one of the generated trial configurations with the probability $P^L_{new} = \frac{exp(-\beta U_2^{p,r})}{W^L_{new}}$ and insert the large molecule.

Based on the two algorithms described above, for the large molecule insertion move, the ratio of the probabilities for generating the move $new\ (N_1^L+1,\ N_1^S-N_{EX};\ N_2^L-1,\ N_2^S+N_{EX}) \rightarrow old\ (N_1^L, N_1^S; N_2^L, N_2^S)$ to that of the reverse move is:

$$\frac{\alpha(new\rightarrow old)}{\alpha(old\rightarrow new)} = \frac{\frac{1}{N_1^L+1}\times\frac{N_{EX}!N_2^S!}{(N_2^S+N_{EX})!}}{\frac{1}{N_1^S}\times\frac{(N_{EX}-1)!(N_{S,\ VEX}-N_{EX})!}{(N_{S,VEX}-1)!}\times\frac{1}{N_2^L}} \times \frac{\frac{1}{V_2}\times\frac{(N_{EX}-1)!}{V_{EX}^{N_{EX}-1}}}{\frac{N_{EX}!}{V_2^{N_{EX}}}} \times \prod_{i=1}^{N_{EX}}\left(\frac{P^S_{i,old}}{P^S_{i,new}}\right)\times\frac{P^L_{old}}{P^L_{new}} \tag{8}$$

where, $N_{S,VEX}$ is the number of small kind molecules found within the exchange sub-volume (V_{EX}). Simplifying Eq. (8) and substituting into Eq. (3), produces the acceptance criteria for the large molecule insertion and small molecule(s) deletion in box 1.

$$acc(old\rightarrow new) = min\left\{1\ ,\ \frac{N_2^L N_1^S}{N_1^L+1} \times \frac{(N_{S,VEX}-1)!N_2^S!}{\left(N_2^S+N_{EX}\right)!(N_{S,\ VEX}-N_{EX})!}\times\left(\frac{V_2}{V_{EX}}\right)^{N_{EX}-1} \times \prod_{i=1}^{N_{EX}}\left(\frac{W^S_{i,new}}{W^S_{i,old}}\right)\times\frac{W^L_{new}}{W^L_{old}}\right\} \tag{9}$$

For the large molecule deletion move, the ratio of the probabilities for generating the move $new\ (N_1^L-1,\ N_1^S+N_{EX};\ N_2^L+1,\ N_2^S-N_{EX}) \rightarrow old\ (N_1^L, N_1^S; N_2^L, N_2^S)$ to that of the reverse move is:

$$\frac{\alpha(new\rightarrow old)}{\alpha(old\rightarrow new)}=\frac{\frac{1}{N_2^L+1}\times\frac{1}{N_1^S+N_{EX}}\times\frac{(N_{EX}-1)!N_{S,\,VEX}!}{(N_{S,\,VEX}+N_{EX}-1)!}}{\frac{1}{N_1^L}\times\frac{N_{EX}!(N_2^S-N_{EX})!}{N_2^S!}}\times\frac{\frac{N_{EX}!}{V_2^{N_{EX}}}}{\frac{1}{V_2}\times\frac{(N_{EX}-1)!}{V_{EX}^{N_{EX}-1}}}\times\prod_{i=1}^{N_{EX}}\left(\frac{P_{i,old}^S}{P_{i,new}^S}\right)\times\frac{P_{old}^L}{P_{new}^L} \tag{10}$$

Simplifying Eq. (10) and substituting into Eq. (3), produces the acceptance criteria for the large molecule deletion and small molecule(s) insertion in box 1.

$$acc(old\rightarrow new)=min\left\{1\ ,\ \frac{N_1^L}{\left(N_2^L+1\right)\left(N_1^S+N_{EX}\right)}\times\frac{N_{S,VEX}!N_2^S!}{\left(N_2^S-N_{EX}\right)!(N_{S,\,VEX}+N_{EX}-1)!}\times\left(\frac{V_{EX}}{V_2}\right)^{N_{EX}-1}\times\prod_{i=1}^{N_{EX}}\left(\frac{W_{i,new}^S}{W_{i,old}^S}\right)\times\frac{W_{new}^L}{W_{old}^L}\right\} \tag{11}$$

The energy difference between configuration *new* and *old*, does not appear directly in the acceptance criteria because their Boltzmann weight is already included in the probabilities used for selecting the position of the molecules.

For $N_{EX}=1$, the acceptance criteria given in Eqs. (9) and (11), simplifies to that of the standard identity-exchange acceptance move [25,26].

$$acc\left(N_1^L,N_1^S;N_2^L,N_2^S\rightarrow N_1^L+1,\ N_1^S-1;\ N_2^L-1,\ N_2^S+1\right)=min\left\{1\ ,\ \frac{N_2^LN_1^S}{\left(N_1^L+1\right)\left(N_2^S+1\right)}\times\frac{W_{new}^L}{W_{old}^L}\ \times\frac{W_{new}^S}{W_{old}^S}\right\} \tag{12}$$

$$acc\left(N_1^L,N_1^S;N_2^L,N_2^S\rightarrow N_1^L-1,\ N_1^S+1;\ N_2^L+1,\ N_2^S-1\right)=min\left\{1\ ,\ \frac{N_1^LN_2^S}{\left(N_2^L+1\right)\left(N_1^S+1\right)}\times\frac{W_{new}^L}{W_{old}^L}\ \times\frac{W_{new}^S}{W_{old}^S}\right\} \tag{13}$$

2.2. Molecular exchange Monte Carlo, version 3 (ME-3)

The major difference between the ME-2 and ME-3 algorithms is that while ME-2 uses a rigid body insertion, in the ME-3 algorithm, the molecules to be exchanged are grown bead by bead using the coupled-decoupled configurational-bias Monte Carlo (CD-CBMC) algorithm [5]. The forward to reverse probability ratios for generating the large molecule insertion and the large molecule deletion moves are identical to those given in Eqs. (8) and (10), respectively. The acceptance criteria for the ME-3 algorithm is identical to that of ME-2 given by Eqs. (9) and (11). An illustration of the large molecule insertion and deletion in box 1 in ME-3 algorithm is provided in Figs. S1 and S2, respectively.

3. Force fields

Calculations were performed with the Transferable Potentials for Phase Equilibria (TraPPE) [27,28] and the Mie potentials of Potoff et al. [29,30]. Both TraPPE and the Mie potentials use a similar potential function, which is presented here as an n-6 Mie potential

$$U(r_{ij})=C_n\varepsilon_{ij}\left[\left(\frac{\sigma_{ij}}{r_{ij}}\right)^{n_{ij}}-\left(\frac{\sigma_{ij}}{r_{ij}}\right)^{6}\right]+\frac{q_iq_j}{4\pi\varepsilon_or_{ij}} \tag{14}$$

where r_{ij}, ε_{ij}, and σ_{ij} are the separation, well depth, and collision diameter, respectively, for the pair of interaction sites i and j. Simulations of 1-octanol include electrostatic interactions that are modeled via partial charges. The constant C_n is a normalization factor used such that the minimum of the potential remains at $-\varepsilon_{ij}$ for all n_{ij}.

$$C_n=\left(\frac{n_{ij}}{n_{ij}-6}\right)\left(\frac{n_{ij}}{6}\right)^{6/(n_{ij}-6)} \tag{15}$$

For $n=12$, the standard 12-6 Lennard-Jones potential used by TraPPE is recovered. Parameters governing interactions between unlike interaction sites were determined using the Lorentz-Berthelot combining rules [31,32].

$$\sigma_{ij}=(\sigma_{ii}+\sigma_{jj})/2 \tag{16}$$

$$\varepsilon_{ij}=\sqrt{\varepsilon_{ii}\varepsilon_{jj}} \tag{17}$$

To determine repulsion exponents for cross interactions, an arithmetic average was used [33].

$$n_{ij}=(n_{ii}+n_{jj})/2 \tag{18}$$

All non-bonded parameters used in this work are listed in Table 1, and were taken from their original sources without modification.

All bonded parameters for alkanes, perfluoroalkanes, and 1-octanol, were taken from previous work [5,24,27–30]. Fixed bond lengths were used to connect pseudo-atoms and are listed in Table 2.

Angle bending was described using a harmonic potential

$$U_{bend}=\frac{k_\theta}{2}(\theta-\theta_0)^2 \tag{19}$$

where θ is the measured bond angle, θ_0 is the equilibrium bond angle, and k_θ is the force constant. Equilibrium bond angles and bending constants are listed in Table 2.

Dihedral energies were represented by a cosine series where φ is

Table 1
Non-bonded parameters for alkanes, perfluoroalkanes, and 1-alcohols.

Model	Pseudo-atom	ε_i/k_b(K)	σ_i (Å)	q_i(e)	n_i
Mie-alkanes [29,30]	CH_4	161.00	3.740	0.000	14
	CH_3	121.25	3.783	0.000	16
	CH_2	61.00	3.990	0.000	16
	CH ($C_N>4$)	14.00	4.700	0.000	16
	C ($C_N>4$)	1.20	6.200	0.000	16
Mie-perfluoroalkanes [24,30]	CF_3	155.75	4.475	0.000	36
	CF_2	72.20	4.750	0.000	44
TraPPE-alkanes [5,27]	CH_4	148.00	3.730	0.000	12
	CH_3	98.00	3.750	0.000	12
	CH_2	46.00	3.950	0.000	12
	CH	10.00	4.680	0.000	12
	C	0.50	6.400	0.000	12
TraPPE-alcohols [28]	CH_3-(OH)	98.00	3.750	0.265	12
	CH_2-(OH)	46.00	3.950	0.265	12
	O	93.00	3.020	−0.700	12
	H	0.00	0.000	0.435	12

Table 2
Equilibrium bond lengths, bond angles, and bending constants for alkanes, perfluoroalkanes, and alcohols. Dihedral energies were represented by a cosine series.

Bond type	Bond length/Å	Angle type	θ_0/degree	k_θ/K-rad^{-2}
$CF_x - CF_y$	1.540	$CF_x - CF_2 - CF_y$	114.00	62500
$CH_x - CH_y$	1.540	$CH_x - CH_2 - CH_y$	114.00	62500
$CH_x - C$	1.540	$CH_x - CH - CH_y$	112.00	62500
$CH_x - O$	1.430	$CH_x - C - CH_y$	109.47	62500
$O - H$	0.945	$CH_x - CH_2 - O$	109.47	50400
		$CH_x - O - H$	108.50	55400

Table 3
Torsional parameters for alkanes, perfluoroalkanes, and alcohols.

Torsion	n	c_n/K	δ_n
CF_x—(CF_2)—(CF_2)—CF_y	0	−1577.68	0
	1	791.61	0
	2	333.65	0
	3	854.01	0
	4	349.25	0
	5	211.51	0
	6	117.66	0
	7	−83.44	0
CH_x—(CH_2)—(CH_2)—CH_y	1	355.03	0
	2	−68.19	180
	3	791.32	0
CH_x—(CH_2)—(CH)—CH_y	0	−251.06	0
	1	428.73	0
	2	−111.85	180
	3	441.27	0
CH_x—(CH_2)—(C)—CH_y	3	461.29	0
CH_x—(CH_2)—(CH_2)—O	1	176.62	0
	2	−53.34	180
	3	769.93	0
CH_x—(CH_2)—(O)—H	1	209.82	0
	2	−29.17	180
	3	187.93	0

the dihedral angle, c_n are dihedral force constants, n is the multiplicity, and δ_n is the phase shift. The cosine series accounts for the total rotational barrier, and no 1–4 Lennard-Jones interactions were included in the model. Fourier constants are listed in Table 3.

$$U_{tors} = \sum_{n=0} c_n[1 + \cos(n\varphi - \delta_n)] \quad (20)$$

4. Simulation Methodology

The molecular exchange Monte Carlo algorithms described in Section 2.1 and 2.2 were implemented for Gibbs ensemble simulations in the development version of GPU Optimized Monte Carlo (GOMC), which is available to the public via GitHub [34]. GOMC is an object-oriented Monte Carlo simulation engine, capable of performing simulations in canonical, isobaric-isothermal, grand canonical ensembles, as well as Gibbs ensemble Monte Carlo. GOMC is designed for the simulation of complex molecular topologies, and supports a variety of potential functions, such as Lennard-Jones and Mie potentials. Coulomb interactions are also supported via the Ewald summation method [35]. GOMC is capable of parallel computation, either on multicore CPUs or GPUs.

Initial configurations were generated with Packmol [36], and Psfgen was used to generate coordinate (*.pdb) and connectivity (*.psf) files [37]. Parameters for the configurational-bias swap move were: 100 angle trials, 100 dihedral trials, 10 trial locations for the first site, and 8 trial locations for secondary sites. In calculations using the MEMC move, the first and last carbon atoms in a molecule were used to define the backbone of the large and small molecules. Non-bonded potentials were truncated at 10 Å and 14 Å for Mie [29,30] and TraPPE [5,27,28] force fields, respectively, and analytical tail corrections were applied to the energy and pressure [29]. For all simulations with polar molecules, the real part of electrostatic potential was truncated at 14 Å and 120 Å for the liquid and vapor phase, respectively, and an Ewald convergence tolerance of 1×10^{-5} was used. For NVT-GEMC simulations, the pressure was calculated with frequency of 1×10^3 MCS.

4.1. Pressure-composition diagrams

The pressure-composition phase diagrams of methane + n-butane and perfluorobutane + n-butane were predicted using NPT-GEMC and NVT-GEMC simulations, respectively. NVT-GEMC simulations were used for the perfluorobutane + n-butane system due to the narrow range of pressures for which vapor-liquid phase coexistence exists at 260 K. Calculations were performed on systems containing 1000 molecules, with a move ratio of 38% displacements, 10% rotations, 2% volume transfers, 10% coupled-decoupled configurational-bias regrowth, 20% MEMC, and 20% coupled-decoupled configurational-bias (CD-CBMC) molecule transfers. 4×10^7 Monte Carlo steps (MCS) were used for equilibration, followed by a data production period of 6×10^7 MCS. Statistical uncertainties were determined from three independent sets of simulations, where each simulation was initiated with a different random number seed. For the MEMC move, an exchange subvolume of 8.8 Å × 8.8 Å x 11.8 Å was used [24].

4.2. Free energies of transfer

To calculate the Gibbs free energies of transfer for n-alkanes (C1–C8) from vapor phase to liquid 1-octanol, n-hexadecane, or 2,2,4-trimethylpentane, the initial vapor phase consisted of 580 methane, 50 ethane, 10 propane, 2 n-butane, 2 n-pentane, 2 n-hexane, 2 n-heptane, and 2 n-octane molecules, packed in a cubic box with side length of 300 Å. The liquid phase contained 240 1-octanol, 150 n-hexadecane or 250 2,2,4-trimethylpentane molecules, packed in cubic box with side length of 30 Å. Each phase was equilibrated for 1×10^7 MCS with isobaric-isothermal (NPT) simulations, with a move ratio of 38% displacements, 20% rotations, 2% volume transfers, 20% CD-CBMC regrowth, and 20% crankshaft [38,39].

Starting from the equilibrated configurations, NPT-GEMC simulations were performed at 298 K and 1 atm pressure, with a move ratio of 29% displacements, 10% rotations, 1% volume transfers, 10% CD-CBMC regrowth, 10% crankshaft, 20% MEMC, and 20% CD-CBMC molecule transfer. Seven large-small molecule pairs were defined for the MEMC move, with an exchange ratio of 1:1: (ethane, methane), (propane, ethane), (n-butane, propane), (n-pentane, n-butane), (n-hexane, n-pentane), (n-heptane, n-hexane), and (n-octane, n-heptane). Pairs were chosen with equal probability to exchange the large molecule with the small molecule in the liquid phase. Each simulation was run for 1×10^8 Monte Carlo steps, and statistical uncertainties were determined from ten independent sets of simulations, where each simulation was initiated with a different random number seed. All molecule types were allowed to be transferred between vapor and liquid phases, except for 1-octanol, n-hexadecane, and 2,2,4-trimethylpentane, due to the very low vapor pressure of these molecules at 298 K.

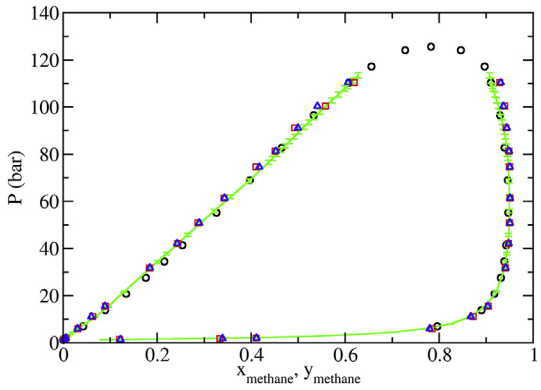

Fig. 3. Pressure composition diagram for methane + n-butane at 277 K predicted from NPT-GEMC simulations using Mie potentials [30]. Experimental data (black circles) [40], GCMC + histogram reweighting [24] (green lines), ME-2 algorithm (red squares), and ME-3 algorithm (blue triangles). Calculations were performed with an exchange ratio of one n-butane with one methane. The uncertainties in the predicted methane mole fractions were less than 0.01 and 0.004 in liquid and vapor phase, respectively.

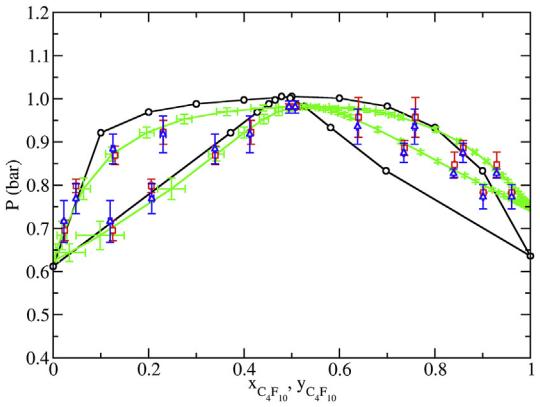

Fig. 4. Pressure-composition diagram for perfluorobutane + n-butane at 260 K predicted from NVT-GEMC simulations using Mie potentials [30]. Experimental data (black circles) [41], GCMC + histogram reweighting (green lines) [24], ME-2 algorithm (red squares), and ME-3 algorithm (blue triangles), with an exchange ratio of one perfluorobutane with one n-butane. The line connecting the experimental data points is provided as a guide to the eye.

5. Results and discussion

In this section, a number of examples are provided to validate the molecular exchange move in GEMC simulations, and to illustrate how the MEMC move can be used to significantly enhance acceptance rates for the molecule transfer move. Binary mixture phase diagrams were calculated for methane + n-butane and perfluorobutane + n-butane. Additional calculations were performed to calculate the Gibbs free energy of transfer for n-alkanes from vapor phase to liquid 1-octanol, n-hexadecane, and 2,2,4-trimethylpentane, to highlight the efficiency of the combination of MEMC and GEMC for the calculation of free energies of transfer.

5.1. Pressure-composition diagrams

In Fig. 3, the pressure vs. composition diagram for methane + n-butane at 277 K, predicted using the ME-2 and the ME-3 algorithm, is compared with prior GCMC + histogram reweighting simulations [24] and experimental [40] data. Interactions between molecules were described with the Optimized Mie Potentials of Potoff et al. [30]. Calculations were performed with an exchange ratio of one n-butane with one methane. In addition to showing excellent agreement with experimental data, GEMC simulations with the ME-2 and ME-3 algorithm produced results that were statistically indistinguishable from prior simulations, validating the method. Additional calculations were performed with an exchange ratio of one n-butane to two methane molecules, and the resulting pressure-composition diagram is shown in Fig. S3.

In Table 4, the average acceptance percentage for molecule transfers as a function of composition in liquid phase is presented for the methane + n-butane mixture at 277 K. When performing a one to one exchange, ME-3 was found to produce the largest improvement in acceptance rates. Acceptance rates for the MEMC move were 3–10 times larger than configurational-bias swaps. The ME-2 algorithm produced acceptance rates that were 2–3 times configurational-bias swaps for $x_{methane} > 0.5$.

Because the ME-2 algorithm uses a rigid swap and the centroid of the large molecule is placed at the geometric center of the exchange sub-volume, only a fraction of the sub-volume is guaranteed to be empty. This is especially true when swapping molecules that differ greatly in size, such as methane and n-butane. In most of the ME-2 exchanges, it is likely that some atoms from the large molecule will have overlaps with existing molecules, lowering acceptance rates compared to ME-3. The ME-3 algorithm uses the same initial placement for the central atom as ME-2, but it grows the rest of the large molecule using configurational-bias. This allows the algorithm to find more energetically favorable configurations than are possible through a rigid molecule insertion, leading to greater acceptance rates for the exchange move in this system.

When performing a one to two exchange for methane + n-butane, ME-3 was found to produce up to a factor of three times improvement in acceptance rates at $x_{methane} = 0.95$, while the ME-2 algorithm produced acceptance rates similar to configurational-bias swaps. For all methane compositions, the acceptance rate for

Table 4
Average acceptance percentages for molecule swaps of n-butane and perfluorobutane in GEMC simulations of methane + n-butane and perfluorobutane + n-butane, respectively.

Binary system	Sub-volume size (Å)	N_{EX}	$x^{liquid}_{C_4H_{10}}$	$x^{vapor}_{C_4H_{10}}$	CD-CBMC	ME-2	ME-3
methane + n-butane	–	1	0.50	0.05	2.56	3.15	7.68
			0.75	0.05	0.87	1.67	5.53
			0.95	0.13	0.45	1.24	4.34
	8.8 × 8.8 × 11.8	2	0.50	0.05	2.56	2.30	4.63
			0.75	0.05	0.87	1.12	2.88
			0.95	0.13	0.45	0.44	1.27
perfluorobutane + n-butane	–	1	0.14	0.27	0.112	5.267	3.832
			0.51	0.49	0.068	4.696	3.024
			0.87	0.66	0.018	3.675	1.887

a one to two exchange is less than a one to one exchange due to the difficulty in finding two methane molecules within the exchange sub-volume.

In Fig. 4, the pressure vs. composition diagram for perfluorobutane + n-butane at 260 K, predicted using GEMC simulations with the ME-2 and ME-3 algorithm is shown. Simulations were performed with the Mie potentials [30], which include an update to the perfluorocarbon force field [24]. The predictions of GEMC simulations are in close agreement with prior GCMC + histogram-reweighting calculations [24], validating the algorithm and its implementation in GOMC. Using standard Lorentz-Berthelot combining rules [31,32] and no adjustable parameters for the cross interaction, very good agreement was achieved with experiment [41]. The largest deviation results from the limitation in the united-atom force field for perfluorobutane, which over-predicts the vapor pressure at 260 K by approximately 0.1 bar.

In Table 4, the average acceptance percentages for molecule transfers as a function of composition in liquid phase are presented for the perfluorobutane + n-butane mixture at 260 K. Using coupled-decoupled configurational-bias (CD-CBMC) swaps, the probability of successfully inserting one perfluorobutane into the liquid phase, containing 14 mol%, 51 mol%, and 87 mol% of n-butane was 0.112%, 0.068%, and 0.018%, respectively. For the ME-2 algorithm, depending on composition, acceptance rates for the transfer of perfluorobutane were 47–204 times greater than CD-CBMC, while for ME-3, acceptance rates were 34–105 times greater than CD-CBMC. The MEMC move has approximately twice the computational cost of a standard CD-CBMC swap move, and therefore provides substantial improvements in computational efficiency. For an extensive discussion of the computational efficiency of the MEMC algorithm readers are directed to Ref. [24]. For this system, the ME-2 algorithm produces the largest acceptance rates because it works by aligning the backbone of perfluorobutane with the cavity left by the leaving n-butane and, in this case, the two molecules to be exchanged have similar size and shape. Acceptance rates were slightly lower for ME-3, since it grows the molecule using coupled-decoupled configurational-bias, without requiring the backbone of the molecule to be aligned with the cavity created by the molecule that was removed.

5.2. Free energies of transfer

Understanding the partitioning of compounds between phases is important for a wide variety of applications, such as drug design [42–44], design of separation processes [45], and prediction of environmental fate of toxic industrial chemicals [46,47]. The most widely used partition coefficient describes the distribution of a solute between 1-octanol and water, which may be determined from the differences in the Gibbs free energies of hydration ΔG_{hyd} and solvation in 1-octanol ΔG_{solv}.

$$\log K_{OW} = \frac{\Delta G_{hyd} - \Delta G_{solv}}{2.303RT} \tag{21}$$

Therefore, it is possible to determine log K_{ow}, and other partition coefficients, directly from computer simulations as long as a suitable methodology exists for the determination of ΔG.

The most common method to calculate free energy changes from atom-based computer simulations is to use molecular dynamics simulations coupled with techniques, such as thermodynamic integration (TI) [44,48–50], free energy perturbation (FEP) [51,52], or adaptive biasing force (ABF) [53–56]. To achieve reliable sampling, these methods require the reaction coordinate to be divided into multiple smaller windows, where each window corresponds to a specific scaling of the Lennard-Jones and electrostatic interactions. Depending on the techniques used, and the level of accuracy desired, the number of discrete windows may vary from 16 [57] to over 60 [50,58]. Typical simulation run lengths vary from 2 to 10 ns per window [50].

Alternatively, recognizing that the Gibbs free energy of transfer could be calculated from the average number density of the solute in each phase [59], Martin and Siepmann proposed an elegant and computationally efficient means for calculating free energies of transfer using Gibbs ensemble Monte Carlo simulations [20].

$$\Delta G_i^{transfer} = -RT\ ln\left(\frac{<\rho_i^{liquid}>}{<\rho_i^{gas}>}\right)_{eq} \tag{22}$$

where, R and T are the molar gas constant and absolute temperature in K, respectively, $<\rho_i^{liquid}>$ and $<\rho_i^{gas}>$ are the ensemble averaged number density (molecule/Å^3) for solute i in liquid and gas phase at equilibrium, respectively. This methodology was used to determine air-water, air-octanol and water-octanol free energies of transfer for alkanes and alcohols with four or fewer carbons using the OPLS [60] and TraPPE [61] force fields.

A critical issue in the use of Gibbs ensemble Monte Carlo for the calculation of free energies of transfer is achieving sufficient numbers of molecule transfers between phases. In the past, this has been addressed by application of the “swatch” move, used extensively by Siepmann and co-workers [20], and more recently by inclusion of continuous fractional component methods [62]. In this section, the effectiveness of the combination of GEMC and the MEMC move is demonstrated through calculations of free energies of transfer of n-alkanes from vapor into liquid 1-octanol, n-hexadecane, and 2,2,4-trimethylpentane.

The octanol-air partition coefficient is used in environmental fate modeling [63], and has been shown to correlate well with air-soil [64,65] and air-particle partitioning [66]. In Fig. 5, the free energies of transfer for n-alkanes (C1–C8) from vapor to liquid 1-octanol at 298 K and 1 atm are shown. Tabulated values of the free energies are listed in Table 5. GEMC calculations were performed with the ME-2 and ME-3 algorithms, and the TraPPE force field [27,28]. The predicted free energies of solvation are in close agreement with experiment [67] and prior calculations using molecular dynamics and the adaptive biasing force method [68]. The results also agree with prior molecular dynamics simulations using

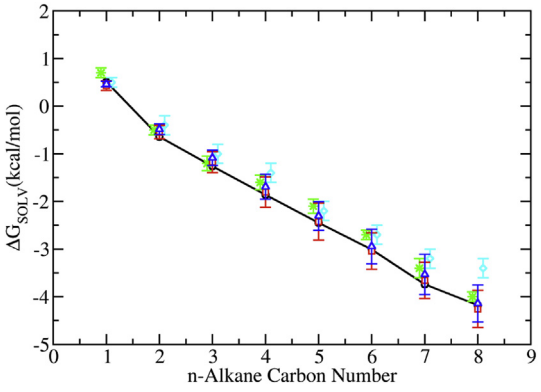

Fig. 5. Free energy of solvation for n-alkanes in liquid 1-octanol predicted from NPT-GEMC simulations at 298 K and 1 atm using the TraPPE forcefield [27,28]. Experimental data (black circles) [67], adaptive biasing force (green stars) [68], thermodynamic integration (cyan diamonds) [57], ME-2 algorithm (red squares), and ME-3 algorithm (blue triangles). The line connecting the experimental data points is provided as a guide to the eye. The TI and ABF data points are shifted slightly along the x-axis for clarity.

Table 5
Free energies of transfer for n-alkanes from gas phase to liquid 1-octanol at 298 K and 1 atm calculated with the TraPPE force field [27,28]. Number in parenthesis corresponds to the statistical uncertainties in the last digit determined from ten independent simulations.

	Free energy of solvation (kcal/mol)					
Solute \ Method	ME-2	ME-3	ABF [68]	TI [57]	GEMC [61]	Experiment [67]
methane	0.44 (11)	0.46 (06)	0.70 (10)	0.5 (1)	0.44 (1)	0.51
ethane	−0.54 (16)	−0.49 (11)	−0.50 (10)	−0.4 (2)	−0.54 (2)	−0.64
propane	−1.18 (22)	−1.09 (16)	−1.20 (15)	−1.0 (2)	−1.18 (2)	−1.26
n-butane	−1.82 (29)	−1.70 (25)	−1.60 (15)	−1.4 (2)	−1.82 (2)	−1.86
n-pentane	−2.42 (35)	−2.31 (30)	−2.10 (15)	−2.2 (2)	–	−2.45
n-hexane	−3.02 (35)	−2.94 (35)	−2.70 (10)	−2.7 (2)	–	−3.01
n-heptane	−3.63 (37)	−3.52 (41)	−3.40 (20)	−3.2 (2)	–	−3.74
n-octane	−4.25 (40)	−4.13 (39)	−4.00 (10)	−3.4 (2)	–	−4.18

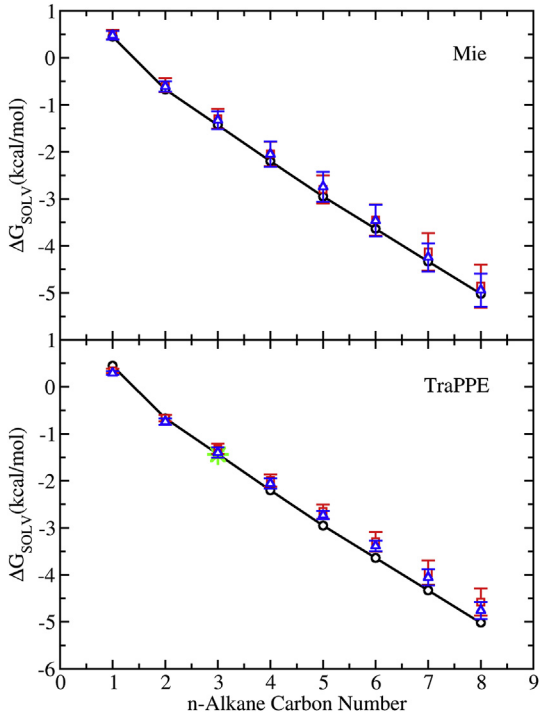

Fig. 6. Free energies of solvation for n-alkanes in liquid n-hexadecane at 298 K and 1 atm predicted from NPT-GEMC simulations using TraPPE [27] and Mie [30] potentials. Experimental data (black circles) [67], thermodynamic integration (green stars) [72], ME-2 algorithm (red squares), and ME-3 algorithm (blue triangles). The line connecting the experimental data points is provided as a guide to the eye.

thermodynamic integration (TI) for methane through hexane, but differences of up to 0.7 kcal/mol in ΔG_{solv} were observed for n-octane [57]. The trend in the data suggests that the TI generated free energy data for longer alkanes in 1-octanol may not have been adequately converged.

The air-hexadecane partition coefficient provides a measurement of non-specific interactions between molecules and plays an important role as a compound descriptor used in linear solvation energy relationships (LSER). LSER models are used for prediction of solute partitioning in a variety of process, providing data that are needed for transport and environmental fate modeling [69,70].

Free energies of solvation for n-alkanes (C1−C8) in liquid n-hexadecane ΔG_{C16} at 298 K and 1 atm, predicted using the TraPPE [27] and Mie [30] force fields, are shown in Fig. 6. Tabulated numerical data are provided in Table 6. The predicted free energies of solvation using the Mie potential are in excellent agreement with experiment [67]. Predictions of the TraPPE force field are in close agreement with experiment for methane through n-butane, however, for longer alkanes TraPPE over-predicts ΔG_{C16} by up to 0.4 kcal/mol for n-octane, which is consistent with prior work [71].

Like the air-hexadecane partition coefficient, the air-2,2,4-trimethylpentane partition coefficient provides a measurement of non-specific solute-solvent interactions. In this case, calculations are performed to demonstrate the consistency of parameterization and transferability of potential parameters for the TraPPE and Mie force fields. Free energies of solvation for n-alkanes (C1−C8) in liquid 2,2,4-trimethylpentane at 298 K and 1 atm, predicted using the TraPPE [5] and Mie [29] force fields, are shown in In Fig. 7. Tabulated numerical data are provided in Table 6. The predicted free energies of solvation using the Mie potential are in excellent agreement with experiment for all solutes [67], while TraPPE force field over-predicts the free energy of solvation by 0.5 kcal/mol for n-octane. The reported experimental value for the free energy of

Table 6
The free energies of transfer for n-alkanes from gas phase to liquid n-hexadecane and 2,2,4-trimethylpentane at 298 K and 1 atm. Calculations were performed with the TraPPE [5,27] and Mie [29,30] potentials. Number in parenthesis corresponds to the statistical uncertainties in the last digit determined from ten independent simulations.

	Free energy of solvation (kcal/mol)									
Solvent	n-hexadecane					2,2,4-trimethylpentane				
Force field	TraPPE		Mie		Expt [67].	TraPPE		Mie		Expt.
Solute	ME-2	ME-3	ME-2	ME-3	–	ME-2	ME-3	ME-2	ME-3	–
methane	0.34 (05)	0.29 (04)	0.50 (10)	0.48 (09)	0.45	0.04 (03)	0.03 (02)	0.10 (04)	0.07 (03)	–
ethane	−0.67 (07)	−0.74 (07)	−0.58 (15)	−0.61 (11)	−0.67	−0.94 (04)	−0.95 (04)	−0.95 (06)	−1.00 (05)	–
propane	−1.32 (11)	−1.40 (11)	−1.30 (21)	−1.33 (19)	−1.43	−1.62 (06)	−1.63 (05)	−1.70 (08)	−1.75 (08)	−1.61
n-butane	−1.99 (13)	−2.06 (11)	−2.05 (26)	−2.05 (27)	−2.20	−2.31 (06)	−2.32 (07)	−2.47 (09)	−2.51 (10)	–
n-pentane	−2.66 (15)	−2.73 (09)	−2.80 (30)	−2.74 (32)	−2.95	−2.98 (06)	−3.00 (09)	−3.20 (12)	−3.25 (12)	−3.21
n-hexane	−3.30 (21)	−3.39 (11)	−3.45 (33)	−3.46 (34)	−3.64	−3.64 (08)	−3.65 (10)	−3.90 (16)	−3.95 (16)	−3.08
n-heptane	−3.95 (26)	−4.05 (17)	−4.13 (40)	−4.25 (30)	−4.33	−4.28 (08)	−4.32 (11)	−4.59 (25)	−4.62 (21)	–
n-octane	−4.58 (29)	−4.76 (18)	−4.86 (46)	−4.94 (35)	−5.02	−4.92 (09)	−4.98 (10)	−5.27 (34)	−5.33 (30)	−5.44

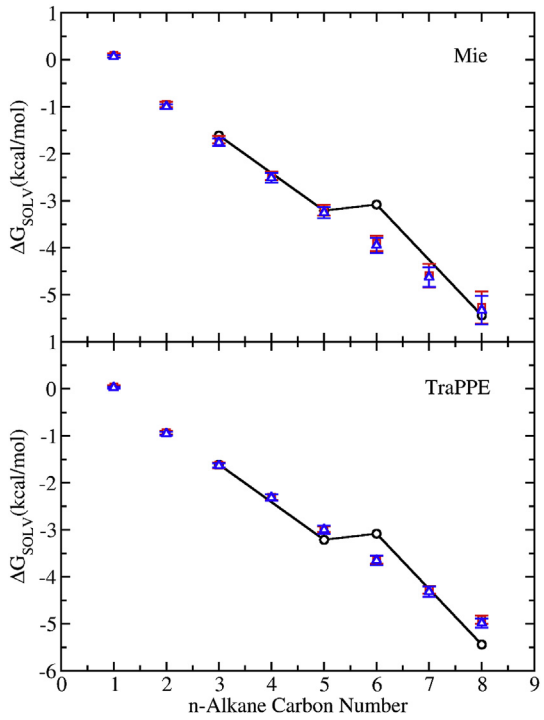

Fig. 7. Free energies of solvation for n-alkanes in liquid 2,2,4-trimethylpentane at 298 K and 1 atm predicted from NPT-GEMC simulations using TraPPE [5] and Mie [29] force fields. Experimental data (black circles) [67], ME-2 algorithm (red squares), and ME-3 algorithm (blue triangles). The line connecting the experimental data points is provided as a guide to the eye.

solvation for n-hexane does not follow the trend of other alkanes, and appears to be erroneous. The calculated free energy of solvation for n-hexane, using the SM5.42R/PM3 solvation model, was found to be −4.14 kcal/mol [67], which is consistent with the trends predicted by simulation. Considering that the SM5.42R/PM3 solvation model under-predicts the experimental solvation free energies of n-pentane and n-octane by 0.19 kcal/mol, it can be assumed that the experimental free energy of solvation for n-hexane should be around −3.95 kcal/mol, which is in exact agreement with the predictions of the Mie potentials.

In Table 7, the average acceptance percentage for insertion/deletion of n-alkane solutes in liquid 1-octanol, n-hexadecane, and 2,2,4-trimethylpentane phase is presented for coupled-decoupled configurational-bias swap, ME-2, and ME-3 methods using the TraPPE potential [5,27,28]. Additional data for the average acceptance percentage for insertion/deletion of n-alkane solutes in liquid n-hexadecane and 2,2,4-trimethylpentane phase, using Mie potential [29,30], are presented in Table S1. As expected, the direct transfer of the solute from gas to liquid phase using the coupled-decoupled configurational-bias method decreases as the solute size increases. The methane transfer acceptance percentage in 1-octanol, n-hexadecane, and 2,2,4-trimethylpentane is 1.73%, 2.02%, and 5.41%, respectively, while the n-octane transfer acceptance percentage is near zero in each solvent. Due to the near zero acceptance rate for transferring solutes longer than n-butane, the insertion/deletion of these molecules depends completely on the MEMC move, which swaps n-butane for n-pentane, n-pentane for n-hexane, n-hexane for n-heptane, n-heptane for n-octane, and vice versa. For all solute exchange pairs, ME-2 algorithm acceptance percentages are 2–10X higher than ME-3 algorithm, except for methane-ethane exchange pair, where ME-3 acceptance percentages are larger than ME-2. The greater acceptance rate for ME-2 vs. ME-3 can be attributed to the use of a rigid body insertion and rotation, which avoids the need to regrow the entire molecule. While regrowing the molecule helps find favorable regions for the molecule, growths can fail if the intramolecular geometric constants (angle bending and dihedral rotation) are not satisfied. Modification of the configurational-bias algorithm to use a Jacobian-Gaussian scheme for the generation of bond angles, for example, may lead to improved acceptance rates for the ME-3 algorithm [7].

In Fig. 8, the effect of run length on the statistical uncertainties of the free energies of transfer is shown as a function of number of

Table 7
Average solute transfer acceptance percentages in GEMC simulations for mixtures of n-alkane +1-octanol, +n-hexadecane, and +2,2,4-trimethylpentane, using the TraPPE potential [5,27,28]. The coupled-decoupled configurational-bias swap acceptance percentages are presented for the small solute swap. The acceptance percentages for ME-2 and ME-3 are for exchanging a small solute with a large one.

Solvent	Solute (small)	Solute (large)	CD-CBMC	ME-2	ME-3
1-octanol	methane	ethane	1.7260	9.1609	13.5644
	ethane	propane	0.7913	7.1385	3.8629
	propane	n-butane	0.1575	3.5902	1.1005
	n-butane	n-pentane	0.0528	2.9461	0.6285
	n-pentane	n-hexane	0.0211	4.5830	0.6617
	n-hexane	n-heptane	0.0078	4.7709	0.6131
	n-heptane	n-octane	0.0026	3.0222	0.2565
	n-octane	–	0.0007	–	–
n-hexadecane	methane	ethane	2.0225	11.5058	19.8150
	ethane	propane	0.9813	9.4266	6.4551
	propane	n-butane	0.2083	4.7896	2.0233
	n-butane	n-pentane	0.0720	3.9912	1.1219
	n-pentane	n-hexane	0.0282	5.8574	1.0091
	n-hexane	n-heptane	0.0097	5.1392	0.6763
	n-heptane	n-octane	0.0026	2.6326	0.2237
	n-octane	–	0.0006	–	–
2,2,4-trimethylpentane	methane	ethane	5.4096	18.2207	28.1561
	ethane	propane	3.2777	15.3756	11.5313
	propane	n-butane	1.0048	8.6308	4.3540
	n-butane	n-pentane	0.4399	7.3336	2.5794
	n-pentane	n-hexane	0.2166	9.6328	2.0855
	n-hexane	n-heptane	0.0879	6.8203	1.1186
	n-heptane	n-octane	0.0268	2.7057	0.2887
	n-octane	–	0.0062	–	–

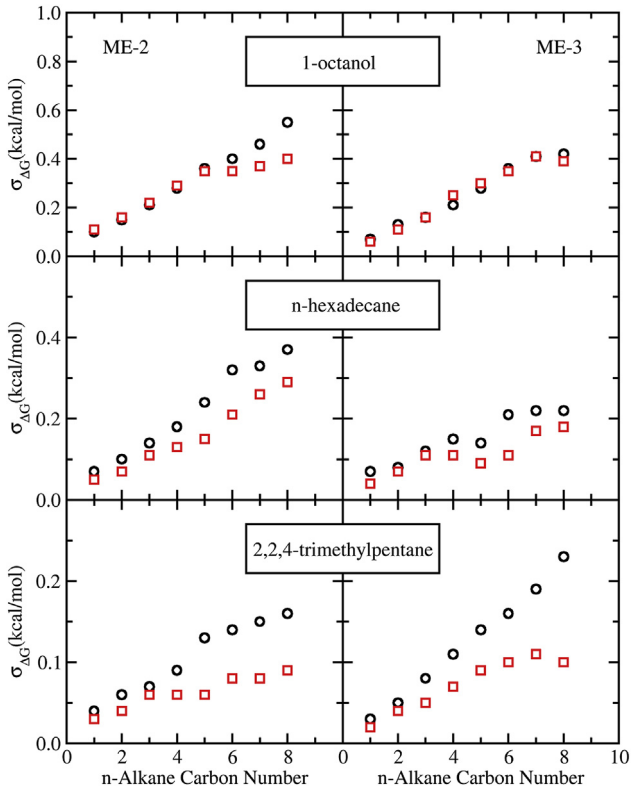

Fig. 8. Standard deviation of predicted free energies of transfer for simulations of 5×10^7 Monte Carlo steps (black circles) and 1×10^8 Monte Carlo steps (red squares).

carbon atoms for both the ME-2 and ME-3 methods. Calculations were performed with the TraPPE force field. In most cases, the ME-3 method produces lower statistical uncertainties for all solutes, despite having lower acceptance rates than the ME-2 method. While greater numbers of molecule identity exchanges occur with ME-2, because ME-3 regrows the solute, the ME-3 method leads to faster sampling of phase space for linear molecules. Only when there is a large difference in acceptance rates does the performance of ME-2 surpass that of ME-3. An example of this is shown for alkane solvation in 2,2,4-trimethylpentane, where ME-2 produces slightly lower statistical uncertainties than ME-3. In this case, acceptance rates for ME-3 were 2–10 times lower than ME-2. For the case of solvation in 1-octanol, for methane to n-butane, the short (5×10^7 Monte Carlo steps) and long simulations (1×10^8 Monte Carlo steps) have similar statistical uncertainties. For molecules longer than butane, increasing the run length by a factor of two reduces the statistical error significantly.

5.3. Evaluation of computational performance

To compare the efficiency of the GEMC-MEMC algorithm as implemented in GOMC with other methods for the calculation of free energies, the solvation free energy for ethane in 1-octanol and n-octane in 2,2,4-trimethylpentane were calculated using GOMC for Monte Carlo, and GROMACS version 2018.2 for thermodynamic integration in molecular dynamic simulations [73]. All calculations were performed on an Intel(R) i5-8600K 3.60 GHz CPU. Calculations in GROMACS followed the protocol given by Garrido et al. [57], and used the same number of solvent molecules in the liquid phase as the Monte Carlo calculations. Lennard-Jones interactions were truncated at 1.0 nm and included dispersion corrections for the energy and pressure. Electrostatic interactions were calculated with the particle mesh Ewald with a converge tolerance of 1E-4. 16 discrete λ values were used, $\lambda \in \left\{ \begin{matrix} 0.0,\ 0.05,\ 0.10,\ 0.20,\ 0.30,\ 0.40,\ 0.50,\ 0.60,\ 0.65, \\ 0.70,\ 0.75,\ 0.80,\ 0.85,\ 0.90,\ 0.95,\ 1.00 \end{matrix} \right\}$, and NVT molecular dynamics simulations of 5 ns in length were performed for each λ value at 298 K. Molecular dynamics simulations were run using 6 CPU-threads and required a total of 50 CPU hours for ethane-1-octanol ($\Delta G_{OA} = -0.54$ kcal/mol) and 35 CPU-hours for n-octane-2,2,4-trimethylpentane ($\Delta G_{224} = -5.00$ kcal/mol). These free energy results are in exact agreement with the predictions of GOMC for the TraPPE force field listed in Tables 5 and 6 The timing data for the molecular dynamics simulations correspond to the free energy calculations, only, and do not include the CPU time required to equilibrate the system. Calculations with GOMC used 4 threads for ethane+1-octanol, and 2 threads for n-octane+2,2,4-trimethylpentane. These calculations generated free energy data for all eight solutes from a single simulation, and required a total of 234 CPU hours for ethane in 1-octanol and 50 CPU hours for n-octane in 2,2,4-trimethylpentane. Considering that Monte Carlo calculations produced data for 8 solutes from a single simulation, while the MD simulations produced only a single data point, the Monte Carlo and molecular dynamics simulations show similar computational performance.

6. Conclusions

The molecular exchange Monte Carlo (MEMC) method has been adapted for use in Gibbs ensemble Monte Carlo simulations. Calculations of pressure-composition diagrams for methane + n-butane and perfluorobutane + n-butane show exact agreement with prior grand canonical Monte Carlo simulations [24]. The combination of GEMC and MEMC was used to predict the free energies of transfer for n-alkanes in 1-octanol, n-hexadecane and 2,2,4-trimethylpentane. In comparison to more traditional methods for the calculation of free energies of solvation (thermodynamic integration in molecular dynamics), the GEMC-MEMC method shows similar computational efficiency. The GEMC-MEMC method has some potential advantages over molecular dynamics simulations for calculation of free energies of solutes which have large energy barriers between conformers. These solutes require either biased sampling techniques or very long molecular dynamics simulations to sample all relevant states [74]. In the GEMC-MEMC, the coupled-decoupled configurational-bias algorithm allows the simulation to rapidly jump between minimum energy conformers, leading to faster sampling of the relevant conformational space.

Free energy calculations for alkanes-1-octanol were performed with only the TraPPE force field, and were in excellent agreement with prior simulations and experimental data. For n-alkane solvation in n-hexadecane and 2,2,4-trimethylpentane, simulations were performed with both the TraPPE and Mie potentials. The Mie potentials were found to offer superior performance compared to TraPPE, being in close agreement with experimental data for all solutes from methane to n-octane. TraPPE displayed good agreement with experiment for n-alkane solutes with four or fewer carbons, but for larger n-alkanes, TraPPE under-predicted free energies of transfer with the difference increasing with solute size.

Acknowledgements

Funding from the National Science Foundation OAC-1642406 is gratefully acknowledged. Some of the computations in this work were performed with resources from the Grid Computing initiative at Wayne State University.

Appendix A. Supplementary data

Supplementary data to this article can be found online at https://doi.org/10.1016/j.fluid.2018.12.032.

References

[1] A.Z. Panagiotopoulos, Direct determination of phase coexistence properties of fluids by Monte-Carlo simulation in a new ensemble, Mol. Phys. 61 (1987) 813–826.
[2] A.Z. Panagiotopoulos, N. Quirke, M. Stapleton, D.J. Tildesley, Phase equilibria by simulation in the Gibbs ensemble - alternative derivation, generalization and application to mixture and membrane equilibria, Mol. Phys. 63 (1988) 527–545.
[3] M. Laso, J.J. De Pablo, U.W. Suter, Simulation of phase-equilibria for chain molecules, J. Chem. Phys. 97 (1992) 2817–2819.
[4] J.I. Siepmann, S. Karaborni, B. Smit, Simulating the critical-behavior of complex fluids, Nature 365 (1993) 330–332.
[5] M.G. Martin, J.I. Siepmann, Novel configurational-bias Monte Carlo method for branched molecules. Transferable potentials for phase equilibria. 2. United-atom description of branched alkanes, J. Phys. Chem. B 103 (1999) 4508–4517.
[6] M.G. Martin, A.L. Frischknecht, Using arbitrary trial distributions to improve intramolecular sampling in configurational-bias Monte Carlo, Mol. Phys. 104 (2006) 2439–2456.
[7] A. Sepehri, T.D. Loeffler, B. Chen, Improving the efficiency of configurational-bias Monte Carlo: extension of the jacobian-Gaussian scheme to interior sections of cyclic and polymeric molecules, J. Chem. Theor. Comput. 13 (2017) 4043–4053.
[8] A. Sepehri, T.D. Loeffler, B. Chen, Improving the efficiency of configurational-bias Monte Carlo: a density-guided method for generating bending angle trials for linear and branched molecules, J. Chem. Phys. 141 (2014).
[9] B. Neubauer, A. Boutin, B. Tavitian, A.H. Fuchs, Gibbs ensemble simulations of vapour-liquid phase equilibria of cyclic alkanes, Mol. Phys. 97 (1999) 769–776.
[10] J.R. Errington, A.Z. Panagiotopoulos, New intermolecular potential models for benzene and cyclohexane, J. Chem. Phys. 111 (1999) 9731–9738.
[11] J.K. Shah, E.J. Maginn, A general and efficient Monte Carlo method for sampling intramolecular degrees of freedom of branched and cyclic molecules, J. Chem. Phys. 135 (2011).
[12] Z. Chen, F.A. Escobedo, A configurational-bias approach for the simulation of inner sections of linear and cyclic molecules, J. Chem. Phys. 113 (2000) 11382–11392.
[13] C.D. Wick, J.I. Siepmann, Self-adapting fixed-end-point configurational-bias Monte Carlo method for the regrowth of interior segments of chain molecules with strong intramolecular interactions, Macromolecules 33 (2000) 7207–7218.
[14] F.A. Escobedo, J.J. Depablo, Monte-carlo simulation of the chemical-potential of polymers in an expanded ensemble, J. Chem. Phys. 103 (1995) 2703–2710.
[15] F.A. Escobedo, F.J. Martinez-Veracoechea, Optimized expanded ensembles for simulations involving molecular insertions and deletions. I. Closed systems, J. Chem. Phys. 127 (2007) 174103.
[16] F.A. Escobedo, Optimized expanded ensembles for simulations involving molecular insertions and deletions. II. Open systems, J. Chem. Phys. 127 (2007) 174104.
[17] W. Shi, E.J. Maginn, Improvement in molecule exchange efficiency in Gibbs ensemble Monte Carlo: development and implementation of the continuous fractional component move, J. Comput. Chem. 29 (2008) 2520–2530.
[18] W. Shi, E.J. Maginn, Continuous fractional component Monte Carlo: an adaptive biasing method for open system atomistic simulations, J. Chem. Theor. Comput. 3 (2007) 1451–1463.
[19] A. Torres-Knoop, N.C. Burtch, A. Poursaeidesfahani, S.P. Balaji, R. Kools, F.X. Smit, K.S. Walton, T.J.H. Vlugt, D. Dubbeldam, Optimization of particle transfers in the Gibbs ensemble for systems with strong and directional interactions using CBMC, CFCMC, and CB/CFCMC, J. Phys. Chem. C 120 (2016) 9148–9159.
[20] M.G. Martin, J.I. Siepmann, Predicting multicomponent phase equilibria and free energies of transfer for alkanes by molecular simulation, J. Am. Chem. Soc. 119 (1997) 8921–8924.
[21] P. Bai, J.I. Siepmann, Assessment and optimization of configurational-bias Monte Carlo particle swap strategies for simulations of water in the Gibbs ensemble, J. Chem. Theor. Comput. 13 (2017) 431–440.
[22] L. Zhang, J.I. Siepmann, Pressure dependence of the vapor-liquid-liquid phase behavior in ternary mixtures consisting of n-alkanes, n-perfluoroalkanes, and carbon dioxide, J. Phys. Chem. B 109 (2005) 2911–2919.
[23] C.D. Wick, J.I. Siepmann, D.N. Theodorou, Microscopic origins for the favorable solvation of carbonate ether copolymers in CO2, J. Am. Chem. Soc. 127 (2005) 12338–12342.
[24] M.S. Barhaghi, K. Torabi, Y. Nejahi, L. Schwiebert, J.J. Potoff, Molecular exchange Monte Carlo: a generalized method for identity exchanges in grand canonical Monte Carlo simulations, J. Chem. Phys. 149 (2018), 072318.
[25] J.J. de Pablo, J.M. Prausnitz, Phase-equilibria for fluid mixtures from Monte-Carlo simulation, Fluid Phase Equil. 53 (1989) 177–189.
[26] A.Z. Panagiotopoulos, Exact calculations of fluid-phase equilibria by Monte-Carlo simulation in a new statistical ensemble, Int. J. Thermophys. 10 (1989) 447–457.
[27] M.G. Martin, J.I. Siepmann, Transferable potentials for phase equilibria. 1. United-atom description of n-alkanes, J. Phys. Chem. B 102 (1998) 2569–2577.
[28] B. Chen, J.J. Potoff, J.I. Siepmann, Monte Carlo calculations for alcohols and their mixtures with alkanes. Transferable potentials for phase equilibria. 5. United-atom description of primary, secondary, and tertiary alcohols, J. Phys. Chem. B 105 (2001) 3093–3104.
[29] J.R. Mick, M.S. Barhaghi, B. Jackman, L. Schwiebert, J.J. Potoff, Optimized Mie potentials for phase equilibria: application to branched alkanes, J. Chem. Eng. Data 62 (2017) 1806–1818.
[30] J.J. Potoff, D.A. Bernard-Brunel, Mie potentials for phase equilibria calculations: application to alkanes and perfluoroalkanes, J. Phys. Chem. B 113 (2009) 14725–14731.
[31] D. Berthelot, Hebd, Seances Acad. Sci 126 (1898) 1703.
[32] H.A. Lorentz, Ueber die Anwendung des Satzes vom Virial in der kinetischen Theorie der Gase, Ann. Phys. 248 (1881) 127–136.
[33] J.R. Mick, M. Soroush Barhaghi, B. Jackman, K. Rushaidat, L. Schwiebert, J.J. Potoff, Optimized Mie potentials for phase equilibria: application to noble gases and their mixtures with n-alkanes, J. Chem. Phys. 143 (2015) 114504.
[34] Y. Nejahi, M. Soroush Barhaghi, J. Mick, B. Jackman, K. Rushaidat, Y. Li, L. Schwiebert, J. Potoff, GOMC, GPU Optimized Monte Carlo for the simulation of phase equilibria and physical properties of complex fluids, SoftwareX 9 (2019) 20–27.
[35] P.P. Ewald, The calculation of optical and electrostatic grid potential, Ann. Phys. 64 (1921) 253–287.
[36] L. Martinez, R. Andrade, E.G. Birgin, J.M. Martinez, PACKMOL: a package for building initial configurations for molecular dynamics simulations, J. Comput. Chem. 30 (2009) 2157–2164.
[37] W. Humphrey, A. Dalke, K. Schulten, VMD: visual molecular dynamics, J. Mol. Graph. Model. 14 (1996) 33–38.
[38] A. Baumgartner, K. Binder, Monte-carlo studies on the freely jointed polymer-chain with excluded volume interaction, J. Chem. Phys. 71 (1979) 2541–2545.
[39] A.J. Pertsin, J. Hahn, H.P. Grossmann, Incorporation of bond-length Constraints in Monte-Carlo simulations of cyclic and linear-molecules - conformational sampling for cyclic alkanes as test systems, J. Comput. Chem. 15 (1994) 1121–1126.
[40] D.G. Elliot, R.J.J. Chen, P.S. Chappele, R. Kobayash, Vapor-liquid-equilibrium of methane-N-butane system at low-temperatures and high-pressures, J. Chem. Eng. Data 19 (1974) 71–77.
[41] J.H. Simons, J.W. Mausteller, The properties of normal-butforane and its mixtures with normal-butane, J. Chem. Phys. 20 (1952) 1516–1519.
[42] C. Hansch, T. Fujita, Rho-sigma-pi analysis . Method for correlation of biological activity + chemical structure, J. Am. Chem. Soc. 86 (1964) 1616–1626.
[43] A. Leo, C. Hansch, D. Elkins, Partition coefficients and their uses, Chem. Rev. 71 (1971) 525–616.
[44] J. Chodera, D. Mobley, M. Shirts, R. Dixon, K. Branson, V. Pande, Alchemical free energy methods for drug discovery: progress and challenges, Curr. Opin. Struct. Biol. 21 (2011) 150–160.
[45] J. Huddleston, A. Veide, K. Kohler, J. Flanagan, S.O. Enfors, A. Lyddiatt, The molecular-basis of partitioning in aqueous 2-phase systems, Trends Biotechnol. 9 (1991) 381–388.
[46] W. Meylan, P. Howard, R. Boethling, D. Aronson, H. Printup, S. Gouchie, Improved method for estimating bioconcentration/bioaccumulation factor from octanol/water partition coefficient, Environ. Toxicol. Chem. 18 (1999) 664–672.
[47] E. Braekevelt, S. Tittlemier, G. Tomy, Direct measurement of octanol-water partition coefficients of some environmentally relevant brominated diphenyl ether congeners, Chemosphere 51 (2003) 563–567.
[48] J.G. Kirkwood, Statistical mechanics of fluid mixtures, J. Chem. Phys. 3 (1935) 300–313.
[49] P. Kollman, Free-energy calculations - applications to chemical and biochemical phenomena, Chem. Rev. 93 (1993) 2395–2417.
[50] M.R. Shirts, J.W. Pitera, W.C. Swope, V.S. Pande, Extremely precise free energy calculations of amino acid side chain analogs: comparison of common molecular mechanics force fields for proteins, J. Chem. Phys. 119 (2003) 5740–5761.
[51] J. Aqvist, Ion water interaction potentials derived from free-energy perturbation simulations, J. Phys. Chem. 94 (1990) 8021–8024.
[52] S.E. Debolt, P.A. Kollman, Investigation of structure, dynamics, and solvation in 1-octanol and its water-saturated solution - molecular-dynamics and free-energy perturbation studies, J. Am. Chem. Soc. 117 (1995) 5316–5340.
[53] J. Henin, C. Chipot, Overcoming free energy barriers using unconstrained molecular dynamics simulations, J. Chem. Phys. 121 (2004) 2904–2914.
[54] J. Henin, G. Fiorin, C. Chipot, M.L. Klein, Exploring multidimensional free energy landscapes using time-dependent biases on Collective variables, J. Chem. Theor. Comput. 6 (2010) 35–47.
[55] E. Darve, A. Pohorille, Calculating free energies using average force, J. Chem. Phys. 115 (2001) 9169–9183.
[56] D. Rodriguez-Gomez, E. Darve, A. Pohorille, Assessing the efficiency of free energy calculation methods, J. Chem. Phys. 120 (2004) 3563–3578.
[57] N.M. Garrido, A.J. Queimada, M. Jorge, E.A. Macedo, I.G. Economou, 1-Octanol/Water partition coefficients of n-alkanes from molecular simulations of

absolute solvation free energies, J. Chem. Theor. Comput. 5 (2009) 2436–2446.
[58] P. Liu, F. Dehez, W.S. Cai, C. Chipot, A toolkit for the analysis of free-energy perturbation calculations, J. Chem. Theor. Comput. 8 (2012) 2606–2616.
[59] A. Ben-Naim, Standard thermodynamics of transfer-uses and misuses, J. Phys. Chem. 82 (1978) 792–803.
[60] B. Chen, J. Siepmann, Partitioning of alkane and alcohol solutes between water and (Dry or wet) 1-Octanol, J. Am. Chem. Soc. 122 (2000) 6464–6467.
[61] B. Chen, J. Siepmann, Microscopic structure and solvation in dry and wet octanol, J. Phys. Chem. B 110 (2006) 3555–3563.
[62] A. Poursaeidesfahani, A. Rahbari, A. Torres-Knoop, D. Dubbeldam, T.J.H. Vlugt, Computation of thermodynamic properties in the continuous fractional component Monte Carlo Gibbs ensemble, Mol. Simulat. 43 (2017) 189–195.
[63] Y. Su, F. Wania, T. Harner, Y. Lei, Deposition of polybrominated diphenyl ethers, polychlorinated biphenyls, and polycyclic aromatic hydrocarbons to a boreal deciduous forest, Environ. Sci. Technol. 41 (2007) 534–540.
[64] M. Hippelein, M. McLachlan, Soil/air partitioning of semivolatile organic compounds. 1. Method development and influence of physical-chemical properties, Environ. Sci. Technol. 32 (1998) 310–316.
[65] K. Goss, J. Buschmann, R. Schwarzenbach, Adsorption of organic vapors to air-dry soils: model predictions and experimental validation, Environ. Sci. Technol. 38 (2004) 3667–3673.
[66] T. Harner, T. Bidleman, Octanol-air partition coefficient for describing particle/gas partitioning of aromatic compounds in urban air, Environ. Sci. Technol. 32 (1998) 1494–1502.
[67] J.B. Li, T.H. Zhu, G.D. Hawkins, P. Winget, D.A. Liotard, C.J. Cramer, D.G. Truhlar, Extension of the platform of applicability of the SM5.42R universal solvation model, Theor. Chem. Acc. 103 (1999) 9–63.
[68] N. Bhatnagar, G. Kamath, I. Chelst, J.J. Potoff, Direct calculation of 1-octanol-water partition coefficients from adaptive biasing force molecular dynamics simulations, J. Chem. Phys. 137 (2012).
[69] G. Bronner, K. Fenner, K.U. Goss, Hexadecane/air partitioning coefficients of multifunctional compounds: experimental data and modeling, Fluid Phase Equil. 299 (2010) 207–215.
[70] A. Stenzel, S. Endo, K.U. Goss, Measurements and predictions of hexadecane/air partition coefficients for 387 environmentally relevant compounds, J. Chromatogr. A 1220 (2012) 132–142.
[71] M. Jorge, N.M. Garrido, C.J.V. Simoes, C.G. Silva, R.M.M. Brito, Predicting hydrophobic solvation by molecular simulation: 1. Testing united-atom alkane models, J. Comput. Chem. 38 (2017) 346–358.
[72] N.M. Garrido, M. Jorge, A.J. Queimada, E.A. Macedo, I.G. Economou, Using molecular simulation to predict solute solvation and partition coefficients in solvents of different polarity, Phys. Chem. Chem. Phys. 13 (2011) 9155–9164.
[73] M.J. Abraham, T. Murtola, R. Schulz, S. Páll, J.C. Smith, B. Hess, E. Lindahl, GROMACS: high performance molecular simulations through multi-level parallelism from laptops to supercomputers, SoftwareX 1–2 (2015) 19–25.
[74] P.V. Klimovich, D.L. Mobley, Predicting hydration free energies using all-atom molecular dynamics simulations and multiple starting conformations, J. Comput. Aided Mol. Des. 24 (2010) 307–316.